

# GroupCDL: Interpretable Denoising and Compressed Sensing MRI via Learned Group-Sparsity and Circulant Attention

Nikola Janjušević<sup>1,3</sup>, Amirhossein Khalilian-Gourtani<sup>2</sup>, Adeen Flinker<sup>2</sup>, Li Feng<sup>3</sup>, Yao Wang<sup>1</sup>

**Abstract**—Nonlocal self-similarity within images has become an increasingly popular prior in deep-learning models. Despite their successful image restoration performance, such models remain largely uninterpretable due to their black-box construction. Our previous studies have shown that interpretable construction of a fully convolutional denoiser (CDLNet), with performance on par with state-of-the-art black-box counterparts, is achievable by unrolling a convolutional dictionary learning algorithm. In this manuscript, we seek an interpretable construction of a convolutional network with a nonlocal self-similarity prior that performs on par with black-box nonlocal models. We show that such an architecture can be effectively achieved by upgrading the  $\ell_1$  sparsity prior (soft-thresholding) of CDLNet to an image-adaptive group-sparsity prior (group-thresholding). The proposed learned group-thresholding makes use of nonlocal attention to perform spatially varying soft-thresholding on the latent representation. To enable effective training and inference on large images with global artifacts, we propose a novel *circulant-sparse attention*. We achieve competitive natural-image denoising performance compared to black-box nonlocal DNNs and transformers. The interpretable construction of our network allows for a straightforward extension to Compressed Sensing MRI (CS-MRI), yielding state-of-the-art performance. Lastly, we show robustness to noise-level mismatches between training and inference for denoising and CS-MRI reconstruction.

**Index Terms**—Deep-learning, interpretable neural network, nonlocal self-similarity, group-sparsity, unrolled network, convolutional dictionary learning, image denoising, compressed-sensing, MRI

## I. BACKGROUND AND INTRODUCTION

NONLOCAL self-similarity (NLSS) of natural images has proven to be a powerful signal prior for classical and deep-learning based image restoration. However, state-of-the-art NLSS deep-learning methods are widely constructed as black-boxes, often rendering their analysis and improvement beholden to trial and error. Additionally, current implementations of the NLSS prior in deep-learning separately process overlapping image windows, falsely neglecting the dependency between these overlaps. Here, we address these two shortcomings of nonlocal deep neural networks (DNNs) from the perspective of interpretable architecture design and sparse array arithmetic. This construction allows us to extend the formulation to compressed sensing magnetic resonance

imaging (CS-MRI) without use of tricks common in adapting black-box methods to inverse-problems.

A growing literature of DNNs, derived as direct parameterizations of classical image restoration algorithms, perform on par with state-of-the-art black-box fully convolutional neural networks, without employing common deep-learning tricks (such as batch-normalization, residual learning, and feature domain processing). This interpretable construction has been shown to be instrumental in obtaining parameter and dataset efficiency [1]–[5]. Our previous work, CDLNet [1], introduced a unique interpretable construction, based on convolutional dictionary learning, and achieved novel robustness to mismatches in observed noise-level during training and inference. In this work, we incorporate the NLSS prior into CDLNet and demonstrate the first instance of an interpretable network bridging the performance gap to state-of-the-art nonlocal black-box methods for image denoising. Additionally, the extension of our method to CS-MRI outperforms existing state-of-the-art methods.

Nonlocal layers in DNNs attempt to model long-range image dependencies by computing pixel-wise self-similarity metrics. To tame the quadratic computational complexity of this operation, image-restoration DNNs generally rely on computing dense similarities on small overlapping patches of the input, which are processed independently by the layer/network and subsequently averaged on overlapping regions to produce the final output [2], [6], [7]. Naturally, such patch-based dense attention may incur a runtime penalty by redundant overlap processing and a restoration penalty due to the disregard for the correlation among these overlapping regions. In this work, we propose a novel circulant-sparse attention operation (CircAtt) that addresses these shortcomings in a computationally efficient manner. CircAtt allows for seamless training and inference on large images, enabling more effective restoration of global degradation such as aliasing-artifacts encountered in CS-MRI.

Previous work used a patch-based group-sparsity prior in an interpretably constructed DNN [2]. However, this approach did not achieve competitive performance with black-box nonlocal DNNs. In contrast, we enforce pixel-wise group-sparsity of a latent convolutional sparse representation, with nonlocal attention performed in a compressed subband domain to aid performance and inference speed. We also propose the novel CircAtt operation, together achieving denoising performance on par with the state-of-the-art methods.

We highlight the following contributions:

<sup>1</sup>New York University Tandon School of Engineering, Electrical and Computer Engineering Department, Brooklyn, NY 11201, USA.

New York University Grossman School of Medicine, <sup>2</sup>Neurology Department, <sup>3</sup>Radiology Department, New York, NY 10016, USA.

Please send all correspondence regarding to this manuscript to N. Janjušević (email:nikola@nyu.edu).

TABLE I: Notation

$\mathbf{x} \in \mathbb{R}^{NC}$	a vector valued image with $N = N_1 \times N_2$ pixels, and vectorized channels, $\mathbf{x} = [\mathbf{x}_1^T, \dots, \mathbf{x}_C^T]^T$ .
$\mathbf{x}_c \in \mathbb{R}^N$	the $c$ -th subband/feature-map/channel of $\mathbf{x}$ .
$\mathbf{x}[n] \in \mathbb{R}^C$	the $n$ -th pixel of $\mathbf{x}$ , $n \in [1, N]$ .
$\mathbf{x}_c[n] \in \mathbb{R}$	the $n$ -th pixel of the $c$ -th channel of $\mathbf{x}$ .
$\vec{n} \in [1, N_1] \times [1, N_2]$	the spatial coordinates of the $n$ -th pixel of $\mathbf{x}$ .
$\mathbf{u} \circ \mathbf{v} \in \mathbb{R}^N$	the element-wise product of two vectors.
$\mathbf{D} \in \mathbb{R}^{NC \times QM}$	a 2D $M$ to $C$ channel synthesis convolution operator with stride $s_c$ , where $Q = N/s_c^2$ .
$\mathbf{D}^T \in \mathbb{R}^{QM \times NC}$	a 2D $C$ to $M$ channel analysis convolution operator with stride $s_c$ , where $Q = N/s_c^2$ .
$\mathbf{U} \in \mathbb{R}^{Q \times N}$	a $Q \times N$ matrix with elements $\mathbf{U}_{ij} \in \mathbb{R}$ .
$\mathbf{U}_{i:} \in \mathbb{R}^N, \mathbf{U}_{:j} \in \mathbb{R}^Q$	the $i$ -th row, $j$ -th column of matrix $\mathbf{U}$ .
$\mathbf{U} \otimes \mathbf{V} \in \mathbb{R}^{QM \times NC}$	Kronecker product of $\mathbf{U} \in \mathbb{R}^{Q \times N}$ and $\mathbf{V} \in \mathbb{R}^{M \times C}$ , i.e. the block matrix with $\mathbf{V}$ s scaled by $\mathbf{U}_{ij} \forall i, j$ .
$\mathbf{I}_N \in \mathbb{R}^{N \times N}$	the $N$ by $N$ identity matrix.
$\mathbf{y} = \mathbf{U}\mathbf{x} \equiv (\mathbf{I}_C \otimes \mathbf{U})\mathbf{x}$	the matrix $\mathbf{U}$ applied channel-wise, i.e. $\mathbf{y}_c = \mathbf{U}\mathbf{x}_c \in \mathbb{R}^Q, \forall 1 \leq c \leq C$ .
$\mathbf{y} = \mathbf{V}\mathbf{x} \equiv (\mathbf{V} \otimes \mathbf{I}_N)\mathbf{x}$	the matrix $\mathbf{V}$ applied pixel-wise, i.e. $\mathbf{y}[i] = \mathbf{V}\mathbf{x}[i] \in \mathbb{R}^M, \forall 1 \leq i \leq N$ .
$\mathbf{S} \in \mathbb{R}_W^{N \times N}$	a real-valued $N \times N$ matrix with BCCB sparsity pattern of window size $W$ .

- a novel and efficient nonlocal self-similarity operation (CircAtt) which addresses the modeling and computational shortcomings of common patch-based dense attention implementations.
- a novel thresholding operation, inspired by a group-sparsity prior, which utilizes a reduced channel dimension of the latent space to achieve competitive inference speeds.
- an interpretable nonlocal CNN with competitive denoising and CS-MRI performance to state-of-the-art black-box models.
- an open-source implementation<sup>1</sup> in the Julia programming language [8].

The remainder of the manuscript is organized as follows: in Section II, we introduce the mathematics and notation behind classical convolutional dictionary learning and group-sparse representation. We also provide context for related black-box and interpretable deep-learning methods. In Section III, we introduce our nonlocal CNN derived from group-sparse convolutional dictionary learning, dubbed GroupCDL. We additionally introduce GroupCDL’s extension for CS-MRI reconstruction and detail our novel CircAtt operation. In Section IV, we show experimental results that compare GroupCDL to state-of-the-art deep learning methods for both denoising and CS-MRI reconstruction.

## II. PRELIMINARIES AND RELATED WORK

### A. Dictionary Learning and Group-Sparse Representation

We consider the observation model of additive white Gaussian noise (AWGN),

$$\mathbf{y} = \mathbf{x} + \boldsymbol{\nu}, \quad \text{where } \boldsymbol{\nu} \sim \mathcal{N}(\mathbf{0}, \sigma^2 \mathbf{I}). \quad (1)$$

Here, the ground-truth image  $\mathbf{x} \in \mathbb{R}^{NC}$  is contaminated with AWGN of noise-level  $\sigma$ , resulting in observed image  $\mathbf{y} \in \mathbb{R}^{NC}$ . For convenience and clarity of notation, we denote images in the vectorized form, and any linear operation

<sup>1</sup><https://github.com/nikopj/GroupCDL>,  
<https://github.com/nikopj/CirculantAttention.jl>.

on an image as a matrix vector multiplication (see Table I for details). In implementation, fast algorithms are used and these matrices are not actually formed, except when explicitly mentioned.

We frame our signal-recovery problem in terms of a (given)  $s_c$ -strided convolutional dictionary  $\mathbf{D} \in \mathbb{R}^{NC \times QM}$ , with  $Q = N/s_c^2$ , i.e. the columns of  $\mathbf{D}$  are formed by integer translates of a set of  $M$  (vectorized) 2D convolutional filters, each having  $C$  channels. We assume  $\exists \mathbf{z} \in \mathbb{R}^{QM}$  s.t.  $\mathbf{x} \approx \mathbf{D}\mathbf{z}$ . The rich works of sparse-representation and compressed-sensing provide guarantees based on assumptions of sparsity in  $\mathbf{z}$  and regularity on the columns of  $\mathbf{D}$  [9]. We refer to  $\mathbf{z}$  as our sparse-code, latent-representation, or subband-representation of  $\mathbf{x}$ .

A popular classical paradigm for estimating  $\mathbf{x}$  from an observed noisy  $\mathbf{y}$  is the Basis Pursuit DeNoising (BPDN) model,

$$\underset{\mathbf{z}}{\text{minimize}} \quad \frac{1}{2} \|\mathbf{y} - \mathbf{D}\mathbf{z}\|_2^2 + \lambda\psi(\mathbf{z}), \quad (2)$$

where  $\psi : \mathbb{R}^{QM} \rightarrow \mathbb{R}_+$  is a chosen regularization function. The Lagrange-multiplier term  $\lambda > 0$  provides a trade-off between satisfying observation consistency and obeying the prior-knowledge encoded by  $\psi$ . A popular approach to solving (2) is the proximal-gradient method (PGM) [10], involving the *proximal-operator* of  $\psi$ , defined as

$$\mathbf{prox}_{\tau\psi}(\mathbf{v}) := \arg \min_{\mathbf{x}} \tau\psi(\mathbf{x}) + \frac{1}{2} \|\mathbf{x} - \mathbf{v}\|_2^2, \quad \tau > 0. \quad (3)$$

PGM can be understood as a fixed point iteration involving the iterative application of a gradient-descent step on the observation consistency term of (2) followed by application of the proximal operator of  $\psi$ ,

$$\mathbf{z}^{(k+1)} = \mathbf{prox}_{\tau\psi}(\mathbf{z}^{(k)} - \eta \mathbf{D}^T(\mathbf{D}\mathbf{z}^{(k)} - \mathbf{y})), \quad (4)$$

where  $\tau = \eta\lambda$ , and  $\eta > 0$  is a step-size parameter.

When  $\psi$  is the sparsity-promoting  $\ell_1$ -norm, the proximal operator is given in closed-form by element-wise soft-thresholding [10],

$$\text{ST}_\tau(\mathbf{z}) = \mathbf{z} \circ \left( 1 - \frac{\tau}{|\mathbf{z}|} \right)_+, \quad (5)$$

where  $(\cdot)_+$  denotes projection onto the positive orthant  $\mathbb{R}_+$ . The resulting PGM iterations are commonly referred to as the Iterative Soft-Thresholding Algorithm (ISTA) [10].

More sophisticated priors ( $\psi$ ) can be used to obtain better estimates of our desired ground-truth image by exploiting correlations between “related” image-pixels. One such prior is *group-sparsity*,

$$\psi(\mathbf{z}) = \sum_{i=1}^{M,Q} \sqrt{\sum_{j=1}^Q \Gamma_{ij} \mathbf{z}_m[j]^2} = \|\sqrt{(\mathbf{I}_M \otimes \mathbf{\Gamma})} \mathbf{z}\|_1, \quad (6)$$

where  $\mathbf{\Gamma} \in \mathbb{R}_+^{Q \times Q}$  is a row-normalized adjacency matrix (i.e.  $\|\mathbf{\Gamma}_{i:}\|_1 = 1$ ), and  $\cdot^2$  and  $\sqrt{\cdot}$  are taken element-wise. The  $i$ th adjacency row ( $\mathbf{\Gamma}_{i:}$ ) measures closeness between the  $i$ th latent pixel ( $\mathbf{z}[i]$ ) and every other latent pixel. Hence, group-sparse regularization may be understood as encouraging similar latent-pixels to share the same channel-wise sparsity

pattern, and has been shown to improve denoising performance under classical patch-based sparse coding methods [11], as well as recent interpretably constructed DNNs [2].

In general, the group-sparse regularizer (6) does not have a closed form proximal-operator. Motivated by the operator proposed in [2], we propose an approximate solution, group-thresholding,

$$\text{GT}_\tau(\mathbf{z}; \mathbf{\Gamma}) = \mathbf{z} \circ \left( 1 - \frac{\tau}{\sqrt{(\mathbf{I}_M \otimes \mathbf{\Gamma})\mathbf{z}^2}} \right)_+ \quad (7)$$

Note that the thresholding operator in Lecouat et. al [2] is equivalent to (7) when the adjacency matrix in their formulation is row-normalized. This approximate solution has the desirable property of reducing to element-wise soft-thresholding (5) when  $\mathbf{\Gamma}$  is the identity matrix. From the perspective of deep-learning, GT involves an ‘‘attention’’ operation: a signal transformation via a similarity/adjacency matrix. Black-box attention networks (e.g. transformers) use attention to generate features for the next layer via matrix-vector multiplication. In contrast, GT performs attention to obtain an adjacency weighted signal energy which informs a spatially varying soft-thresholding, i.e. group-thresholding may be rewritten as,

$$\text{GT}_\tau(\mathbf{z}; \mathbf{\Gamma}) = \text{ST}_{\xi|z|}(\mathbf{z}), \quad \xi = \sqrt{(\mathbf{I}_M \otimes \mathbf{\Gamma})\mathbf{z}^2}.$$

The BPDN (2) problem can be made more expressive by opting to learn an optimal dictionary from a dataset of noisy images  $\mathcal{D} = \{\mathbf{y}\}$ . We express the (convolutional) dictionary learning problem as,

$$\underset{\{\mathbf{z}\}, \mathcal{D} \in \mathcal{C}}{\text{minimize}} \sum_{\mathbf{y} \in \mathcal{D}} \frac{1}{2} \|\mathbf{y} - \mathbf{D}\mathbf{z}\|_2^2 + \lambda\psi(\mathbf{z}), \quad (8)$$

where constraint set  $\mathcal{C} = \{\mathbf{D} : \|\mathbf{D}_{:,j}\|_2^2 \leq 1 \forall j\}$  ensures that the regularization term is not rendered useless by an arbitrary scaling of latent coefficients. Solving (8) generally involves alternating sparse-pursuit (ex. (4)) and a dictionary update with fixed sparse-codes (ex. projected gradient descent) [12].

### B. Unrolled and Dictionary Learning Networks

Approaches in [13]–[15] explore the construction of DNNs as unrolled proximal gradient descent machines with proximal-operators that are implemented by a black-box CNN, learned end-to-end. Although these methods contribute to more principled DNN architecture design in image-processing, their use of black-box neural networks, such as UNets [16] and ResNets [17], ultimately side-step the goal of full interpretability. In contrast, our previous work CDLNet [1] introduces a CNN as a direct parameterization of convolutional PGM (4) with an  $\ell_1$  prior, with layers defined as,

$$\begin{aligned} \mathbf{z}^{(0)} &= \mathbf{0}, \quad \text{for } k = 0, 1, \dots, K - 1, \\ \mathbf{z}^{(k+1)} &= \text{ST}_{\tau^{(k)}} \left( \mathbf{z}^{(k)} - \mathbf{A}^{(k)T} (\mathbf{B}^{(k)} \mathbf{z}^{(k)} - \mathbf{y}) \right), \\ \tau^{(k)} &= \tau_0^{(k)} + \hat{\sigma} \tau_1^{(k)}, \quad \hat{\mathbf{x}} = \mathbf{D}\mathbf{z}^{(K)}. \end{aligned} \quad (9)$$

Parameters  $\Theta = \{\mathbf{D}, \{\mathbf{A}^{T(k)}, \mathbf{B}^{(k)}, \tau_0^{(k)}, \tau_1^{(k)}\}_{k=0}^{K-1}\}$  are optimized by back-propagation of a supervised or unsupervised loss function. In this manuscript, we extend the formulation

and direct parameterization of CDLNet by introducing a novel implementation of the group-sparsity prior, embodied in the proposed GroupCDL architecture (see Section III). We also show that the noise-adaptive thresholding of CDLNet, derived from BPDN (2), extends to GroupCDL in both image denoising and joint denoising and CS-MRI (see Section IV-E).

Zheng et. al [18] propose a DNN architecture based on a classical dictionary learning formulation of image denoising. However, this network heavily employs black-box models such as UNets [16] and multi-layer perceptrons (MLPs). Our proposed method differentiates itself by using a direct parameterization of variables present in the classical proximal gradient method (4) with a group-sparsity regularizer (6). This construction offers an alternative to the use of black-boxes, yielding great learned parameter count efficiency, novel generalization capabilities, and easy extensibility.

Directly parameterized dictionary learning networks [1]–[5], [19] have gained some popularity in recent years due to their simple design and strong structural similarities to popular ReLU-activation DNNs. This connection was first established by the seminal work of Gregor et. al [20] in the form of the Learned Iterative Shrinkage Thresholding Algorithm (LISTA). Here, we build upon this literature by proposing a learned approximate proximal operator for the convolutional dictionary learning formulation of a DNN, derived from a group-sparsity prior (see Section III-B). We demonstrate that such a network can compete well with and outperform state-of-the-art methods, without sacrificing interpretability.

Lecouat et. al [2] propose a nonlocal CNN derived from a patch-based dictionary learning algorithm with a group-sparsity prior, dubbed GroupSC. It is well established that the independent processing of image patches and subsequent overlap and averaging (patch-processing) is inherently suboptimal to the convolutional model, due to the lack of consensus between pixels in overlapping patch regions [4]. Our method is in-part inspired by GroupSC, but is adapted to the convolutional sparse coding with groups defined over sliding windows via CircAtt.

### C. Nonlocal Networks

The nonlocal self-similarity prior in image-restoration DNNs is commonly formulated with patch-based dense attention to manage quadratic complexity [2], [6]. Patch overlap is often used to ensure that artifacts do not occur on local-window boundaries. Despite many such networks being formulated as CNNs, their patch-based inference ultimately diminishes the powerful shift-invariance prior and increases computational cost due to additional processing of overlapping regions (see Section III-D).

Liu et. al [21] proposed an alternate form of patch-based dense attention via the Shifted-Window Vision Transformer architecture (SwinViT), demonstrated on image classification, segmentation, and detection tasks. Their so-called Swin attention mechanism makes use of patching without overlap, using alternating ‘‘shifted’’ patch boundaries between patch-based dense attention layers. This allows some cross over of information of neighboring patches [21]. Liu et. al’s ablation

studies considered use of a sliding-window attention mechanism, similar to our CircAtt, but ultimately abandoned it due to similar performance and slower inference compared to Swin attention on their examined tasks. Liang et. al [7] (SwinIR) adapted the SwinViT architecture for image denoising and other restoration tasks with local degradation operators (ex. super-resolution, JPEG artifact removal). Our proposed method re-examines sliding-window attention in the context of image restoration and shows favorable performance over SwinIR in terms of learned parameter count efficiency.

Zamir et. al [22] proposed Restormer, a multi-resolution transformer model for image restoration. They demonstrated results on image denoising and local degradation operator tasks. Restormer’s core (transformer) block does not use nonlocal attention, but instead computes similarities between entire feature maps (known as “transposed attention”). In contrast, the proposed GroupCDL method operates on a single resolution and implements nonlocal attention.

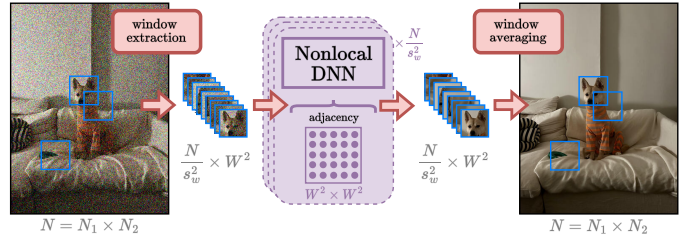
To correctly account for dependencies between neighboring local windows, we propose a sliding-window NLSS (CircAtt), enabled by sparse matrix arithmetic. To the best of our knowledge, we are the first to examine a sliding-window attention mechanism for image restoration. Recent works have proposed other so-called “sparse attention” mechanisms, however, they have either not been in the context of image restoration [23], not employed a sliding-window [24], or have employed a complicated hashing algorithm to exploit extremely long-range dependencies [25].

### III. PROPOSED METHOD

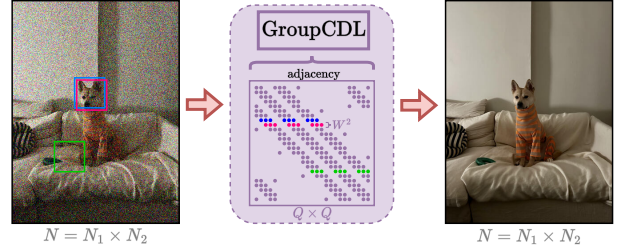
Our proposed framework derives nonlocal attention from the group-sparsity prior (6). We thus begin by introducing our Circulant-Sparse Attention mechanism (Section III-A), which is integral to implementing group-thresholding on convolutional sparse codes, in addition to enabling unified training and inference on large images. In Section III-B, we propose our GroupCDL architecture to tackle the problem of image restoration under the AWGN model (1). AWGN is a popular and successful model for camera noise following white-balance and gamma-correction [26]. Denoising also serves as a fundamental building block (ex. proximal operators) and sub-problem in various inverse-problem approaches [14]. Hence, our proposed method has potential for application beyond camera image denoising. In Section III-C, we demonstrate a significant appeal of interpretable construction by extending the proposed method to Compressed Sensing MRI. Sections III-D and III-E give discussion on the relation between our interpretably constructed nonlocal network and common black-box approaches.

#### A. Circulant-Sparse Attention

The nonlocal self-similarity prior assumes that additional information may be extracted from images by considering different image pixels, patches, or latent pixels, jointly. In practice, for an image with  $N = N_1 \times N_2$  pixels, this prior is implemented via formation of an adjacency matrix  $\Gamma \in \mathbb{R}_+^{N \times N}$  (i.e. a row-normalized similarity matrix), where



(a) Patch-based Dense Attention



(b) Circulant-Sparse Attention (CircAtt)

Fig. 1: (a) To enable dense attention, the input image is divided into overlapping windows (of size  $W \times W$  and with window-stride  $s_w \times s_w$ ), processed independently via a DNN with dense self-attention. The denoised windows are then placed in their original positions and averaged on their overlaps. (b) CircAtt processes the entire image jointly in a single forward pass. The adjacency matrix has a block-circulant with circulant blocks (BCCB) sparsity pattern, where the number of non-zeros in each row/column is at most  $W^2$ . The adjacency matrix is computed in the subband domain, with spatial dimension  $Q = N/s_c^2$ , where  $s_c$  is the convolution stride. Hence, the effective image-domain window-size is  $s_c W \times s_c W$ .

---

#### Algorithm 1: Circulant-Sparse Distance-Similarity

---

```

1 function CircDistSim( $\mathbf{k} \in \mathbb{C}^{Q \times M}$ ,  $\mathbf{q} \in \mathbb{C}^{Q \times M}$ ;  $W \in \mathbb{Z}_+$ ):
2    $S_{ij} = \begin{cases} -\frac{1}{2} \|\mathbf{k}[i] - \mathbf{q}[j]\|_2^2, & \|\vec{i} - \vec{j}\|_\infty \leq W \\ -\infty, & \text{otherwise} \end{cases} \quad \forall (i, j)$ 
3   function bwd( $d\mathbf{S} \in \mathbb{B}_W^{Q \times Q}$ ):
4      $d\mathbf{k} = d\mathbf{S}\mathbf{q} - (d\mathbf{S}\mathbf{1}) \circ \mathbf{k}$ 
5      $d\mathbf{q} = d\mathbf{S}^T \mathbf{k} - (d\mathbf{S}^T \mathbf{1}) \circ \mathbf{q}$ 
6     return  $d\mathbf{k}, d\mathbf{q}$ 
7   return  $\mathbf{S}, \text{bwd}$ 

```

---

the  $i$ th adjacency row ( $\Gamma_{i,:}$ ) measures closeness between a pixel/patch/latent at image position  $i$  and every other image pixel/path/latent. For example, we may reshape a latent representation  $\mathbf{z} \in \mathbb{R}^{N \times C}$  as  $\mathbf{Z} \in \mathbb{R}^{N \times C}$  to compute the dense adjacency  $\Gamma = \text{row-sm}(\mathbf{Z}\mathbf{Z}^T)$ . Here,  $\text{row-sm}$  refers to the softmax function applied row-wise to a matrix,  $\text{row-sm}(\mathbf{S})_{ij} = \frac{e^{S_{ij}}}{\sum_j e^{S_{ij}}}$ .

For computational and memory reasons, it is infeasible to form this dense adjacency matrix even for reasonably small



---

**Algorithm 2: Circulant-Sparse Attention**

---

```

1 function CircAtt ( $\Gamma \in \mathbb{B}_W^{Q \times Q}$ ,  $\mathbf{x} \in \mathbb{C}^{QM}$ ):
2    $\mathbf{y} = \Gamma \mathbf{x}$ 
3   function bwd ( $d\mathbf{y} \in \mathbb{C}^{QM}$ ):
4      $d\Gamma = \text{CircDotSim}(d\mathbf{y}, \mathbf{x}; W)$ 
5      $d\mathbf{x} = \Gamma^T d\mathbf{y}$ 
6     return  $d\Gamma, d\mathbf{x}$ 
7   return  $\mathbf{y}, \text{bwd}$ 

```

---



---

**Algorithm 3: Circulant-Sparse Dot-Similarity**

---

```

1 function CircDotSim ( $\mathbf{k} \in \mathbb{C}^{QM}$ ,  $\mathbf{q} \in \mathbb{C}^{QM}$ ;  $W \in \mathbb{Z}_+$ ):
2    $S_{ij} = \begin{cases} \text{Re}\{\mathbf{q}[j]^H \mathbf{k}[i]\}, & \|i - j\|_\infty \leq W \\ -\infty, & \text{otherwise} \end{cases} \quad \forall (i, j)$ 
3   function bwd ( $d\mathbf{S} \in \mathbb{B}_W^{Q \times Q}$ ):
4      $d\mathbf{k} = d\mathbf{S} \mathbf{q}$ 
5      $d\mathbf{q} = d\mathbf{S}^T \mathbf{k}$ 
6     return  $d\mathbf{k}, d\mathbf{q}$ 
7   return  $\mathbf{S}, \text{bwd}$ 

```

---

image sizes<sup>2</sup>. It is thus common and appropriate to spatially limit our computations to more reasonably sized windows. Ideally, we seek to limit similarity computations for the  $i$ th pixel to pixels  $j$  within a distance  $W$ , i.e. for all  $j$  such that  $\|i - j\| \leq W$  where  $\vec{\cdot}$  notation denotes the conversion from linear to cartesian indexing (see Table I).

Previous architectures have ignored this ideal case for a more practical solution: independently processing overlapping image patches for the entire network [2], [6], or latent patches in each layer [7]. After this processing, image/latent patches may be combined to re-form the image/latent via averaging patches overlapping regions. We illustrate this ‘‘Patch-based Dense Attention’’ in Figure 1a. This patching operation follows arbitrary borders and necessarily neglects dependencies between pixels of neighboring patches, despite their proximity.

We propose a return to the original goal of a spatially-limited nonlocal attention. This goal is achieved by three observations. First, spatially-limited attention defines a Block-Circulant with Circulant Blocks (BCCB) sparsity pattern for the adjacency matrix (when circular boundary conditions are imposed)<sup>3</sup>, as seen illustrated in Figure 1b. As each row of the BCCB-sparse matrix (with window size  $W \times W$ ) contains  $W^2$  elements, the non-zero elements are easily arranged in a matrix  $\tilde{\mathbf{S}} \in \mathbb{R}^{N \times W^2}$ . This sparse matrix may be populated with similarity computations in parallel, and a row-normalization may be performed on  $\tilde{\mathbf{S}}$  using existing fast softmax algorithms.

Second, the now formed BCCB-sparse adjacency matrix may be applied to a vectorized image using existing fast sparse-dense matrix multiplication algorithms.

Third, the back-propagation rules for BCCB-sparse similarity computations and BCCB-sparse attention make use of and maintain the original BCCB sparsity pattern. Memory

<sup>2</sup>Memory and computation scale with side-length to the fourth power. A dense Float32 adjacency matrix for a square images of side lengths 256 and 512 would require 17 and 275 GB of memory, respectively

<sup>3</sup>This is the sparsity pattern of a 2D single-channel convolution matrix

explosion from considering a  $N \times N$  adjacency matrix is not possible, as the sparsity pattern remains fixed. This allows for training with circulant-sparse attention, enabling effective tackling of image restoration with global artifacts/degradation operators, as explored in Section IV-E.

The proposed GroupCDL makes use of a circulant-sparse distance similarity and circulant-sparse attention, detailed in Algorithms 1, 2. In Section IV-D we also consider the use of circulant-sparse dot-product similarity (Algorithm 3), and this algorithm is also necessary during the back-propagation of circulant-sparse attention (regardless of which similarity algorithm is used in the forward pass; see Supplementary Material). In each of these algorithms, a backward-pass function is returned which produces the input gradients (ex.  $d\mathbf{k}, d\mathbf{q}, d\Gamma, d\mathbf{x}$ ) given output gradients (ex.  $d\mathbf{S}, d\mathbf{y}$ ). Derivations of these back-propagation rules are given in the Supplementary Material. Our Circulant-Sparse Attention is implemented in Julia’s CUDA.jl [27] and is publicly available<sup>4</sup>.

### B. The GroupCDL Architecture

We propose a neural network architecture as a direct parameterization of PGM (4) on the convolutional BPDN problem with a group-sparsity prior, dubbed GroupCDL. The GroupCDL architecture is equivalent to replacing the CDLNet [1] architecture’s soft-thresholding (9) with a learned group-thresholding w.r.t an image-adaptive adjacency matrix  $\Gamma$ , as described in Algorithm 5 and shown in Figure 2. Noise-adaptive thresholds are computed using learned parameters  $\tau_0, \tau_1 \in \mathbb{R}_+^M$  (via  $\tau = \tau_0 + \hat{\sigma} \tau_1$ ).  $\mathbf{A}^{T(k)}$ ,  $\mathbf{B}^{(k)}$  are 2D ( $C$  to  $M$  channel, stride- $s_c$ ) analysis and ( $M$  to  $C$  channel, stride- $s_c$ ) synthesis convolutions, respectively.  $\mathbf{D}$  is our 2D ( $M$  to  $C$  channel, stride- $s_c$ ) synthesis convolutional dictionary. For an input noisy image  $\mathbf{y} \in \mathbb{R}^{NC}$ , our latent representation is of the form  $\mathbf{z} \in \mathbb{R}^{QM}$ , where  $Q = N/s_c^2$ .

The adjacency matrix of the group-sparsity prior ( $\Gamma \in \mathbb{R}_+^{Q \times Q}$ ) encodes similarity between latent subband pixels  $\mathbf{z}[i], \mathbf{z}[j] \forall i, j$ . To manage computational complexity while staying true to the convolutional inductive bias of the network, we form this adjacency using a sliding-window of size  $W \times W$  (with circular boundary conditions). Specifically, we compute a circulant-sparse adjacency on a latent representation ( $\mathbf{z}$ ) of the network as

$$\Gamma = \text{row-sm}(\text{CircDistSim}(\overline{\mathbf{W}}_\theta \mathbf{z}, \overline{\mathbf{W}}_\phi \mathbf{z}; W)), \quad (10)$$

via Algorithm 1, where  $\mathbf{W}_\theta, \mathbf{W}_\phi \in \mathbb{R}^{M_h \times M}$  are learned pixel-wise transforms shared across all layers, and  $M_h$  is a hyperparameter. The similarity matrix is normalized via a row-wise softmax operation (**row-sm**). To reduce computational complexity, we only compute similarity every  $\Delta K$  layers. To ensure smooth adjacency matrix updates, a convex combination of the computed adjacency and the adjacency of the previous layer is employed via a learned parameter  $\gamma \in [0, 1]$  (see Alg. 4).

Mimicking the use of subband transforms in the similarity computation (10), we introduce two additional subband

<sup>4</sup><https://github.com/nikopj/CirculantAttention.jl>

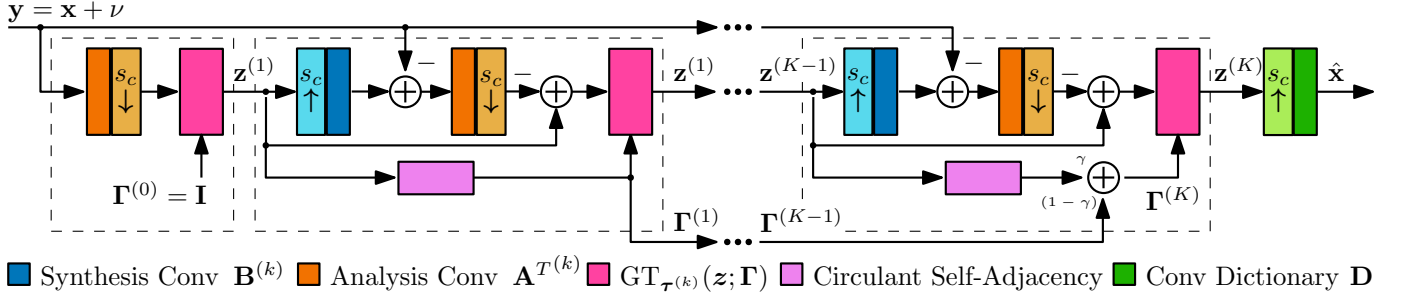


Fig. 2: The GroupCDL Architecture for Denoising: The network begins with no prior of group-sparsity ( $\Gamma^{(0)} = \mathbf{I}$ ). In the second layer, and each subsequent  $\Delta K$  layers, the adjacency matrix  $\Gamma^{(k)}$  is updated by a Circulant(-Sparse) Self-Adjacency computation on the latent representation  $z^{(k)}$ . Expanded views of GT and Circulant Self-Adjacency blocks are given in Fig. 3.

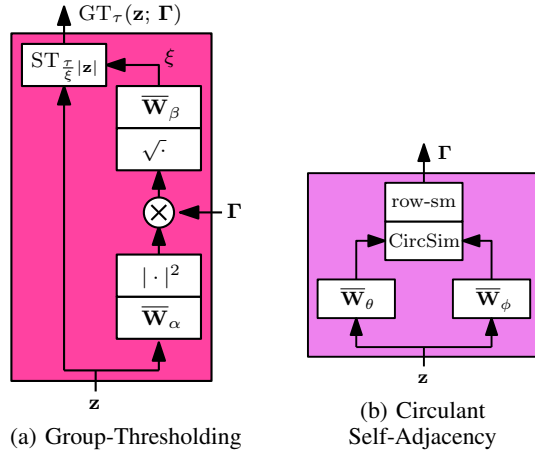


Fig. 3: Expanded block diagrams of GT and Circulant Self-Adjacency from the GroupCDL Architecture (Fig. 2). Group-Thresholding may be viewed as an image-adaptive spatially-varying soft-thresholding, informed by adjacency matrix  $\Gamma$  and the current features.

transforms,  $\mathbf{W}_\alpha \in \mathbb{R}^{M \times M_h}$ ,  $\mathbf{W}_\beta \in \mathbb{R}_+^{M \times M_h}$ , into the group-thresholding operation,

$$\text{GT}_{\tau}(z; \Gamma) = z \circ \left( 1 - \frac{\tau}{\xi} \right)_+, \quad (11)$$

$$\xi = \overline{\mathbf{W}}_\beta \sqrt{(\mathbf{I}_{M_h} \otimes \Gamma)(\overline{\mathbf{W}}_\alpha^T z)^2},$$

where  $\xi \in \mathbb{R}_+^{QM}$  informs an image-adaptive spatially-varying threshold. Here,  $\overline{\mathbf{W}}$  refers to pixel-wise application of a matrix  $\mathbf{W}$  (see Table I). In contrast to (7),  $\mathbf{W}_\alpha$  allows the adjacency-weighted energy of the latent representation to be computed in a compressed subband domain (by setting  $M_h \ll M$ ). Then,  $\mathbf{W}_\beta$  maps this energy back to the uncompressed subband domain ( $M$  channels), pixel-wise. In Section IV-D, we empirically show that the use of a compressed subband domain has a positive impact on denoising performance and an even greater impact on reducing inference time. Figure 3 illustrates the proposed learned group-thresholding operation in block-diagram form.

#### Algorithm 4: Adjacency Matrix Update Forward Pass

```

1 Input:  $\Gamma^{(k-1)}$ ,  $z^{(k)}$ ,  $\gamma \in [0, 1]$ , window-size  $W > 1$ 
2  $\mathbf{S} = \text{CircDistSim}(\overline{\mathbf{W}}_\theta z^{(k)}, \overline{\mathbf{W}}_\phi z^{(k)}; W)$  //Alg. 1
3 if  $k = 1$  then
4    $\Gamma^{(1)} = \text{row-sm}(\mathbf{S})$ 
5 else if  $\text{mod}(k+1, \Delta K) = 0$  then
6    $\Gamma^{(k)} = \gamma \text{row-sm}(\mathbf{S}) + (1-\gamma)\Gamma^{(k-1)}$ 
7 else
8    $\Gamma^{(k)} = \Gamma^{(k-1)}$ 
9 Output:  $\Gamma^{(k)}$ 
    
```

#### Algorithm 5: GroupCDL Denoising Forward Pass

```

1 Input: noisy image  $\mathbf{y}$ , estimated noise-level  $\hat{\sigma}$ 
2 Parameters:
    $\Theta = \{\gamma, \mathbf{W}_{\{\theta, \phi, \alpha, \beta\}}, \mathbf{D}, \{\mathbf{A}^T(k), \mathbf{B}^{(k)}, \tau_{\{0,1\}}^{(k)}\}_{k=1}^{K-1}\}$ 
3 Preprocess:  $\tilde{\mathbf{y}} = \mathbf{y} - \mu$ ,  $\mu = \text{mean}(\mathbf{y})$ 
4 Initialize:  $z^{(0)} = \mathbf{0}$ ,  $\Gamma^{(0)} = \mathbf{I}$ ,  $\tau^{(k)} = \tau_0^{(k)} + \hat{\sigma}\tau_1^{(k)} \forall k$ 
5 for  $k = 0, 1, \dots, K-1$  do
   //Update Adj. using Alg 4
6    $\Gamma^{(k)} \leftarrow \text{AdjUpdate}(\Gamma^{(k-1)}, z^{(k)}, \gamma)$ 
7    $\mathbf{v} = \mathbf{A}^T(k)(\mathbf{B}^{(k)}z^{(k)} - \tilde{\mathbf{y}})$ 
8    $z^{(k+1)} = \text{GT}_{\tau^{(k)}}(z^{(k)} - \mathbf{v}; \Gamma^{(k)})$  //Eq. (11)
9 Output:  $\hat{\mathbf{x}} = \mathbf{D}z^{(K)} + \mu$ 
    
```

#### C. Extending the GroupCDL Architecture for CS-MRI

Parallel (or multi-coil) compressed sensing magnetic resonance imaging (CS-MRI) may in general be described by the following observation model,

$$\mathbf{y} = \mathbf{M}(\mathbf{F}\mathbf{R}\mathbf{x} + \nu), \quad \nu \sim \mathcal{CN}(0, \overline{\Sigma}). \quad (12)$$

where  $\mathbf{x} \in \mathbb{C}^N$  is the ground-truth image-domain signal and  $\mathbf{y} \in \mathbb{C}^{NC}$  is a complex-valued measurement vector with  $C$ -channels acquired in a masked Fourier domain (where  $C$  is the number of scanner coils). Here,  $\mathbf{M} = \text{diag}(\mathbf{m})$  is channel-wise mask operator with binary mask  $\mathbf{m} \in \{0, 1\}^N$  indicating the position of acquired Fourier domain samples.  $\mathbf{F}$  represents the  $N$ -dimensional DFT matrix, which is applied channel-wise. The coil-sensitivities are encoded in the sensitivity operator  $\mathbf{R} = [\text{diag}(\mathbf{r}_1) \ \dots \ \text{diag}(\mathbf{r}_C)]^T$  via sensitivity map  $\mathbf{r} \in \mathbb{C}^{NC}$ . The acquired samples are well

**Algorithm 6: GroupCDL CS-MRI Forward Pass**

- 1 **Input:** zero-filled Fourier domain  $\mathbf{y}$ , estimated noise-level  $\hat{\sigma}$ , Fourier domain mask operator  $\mathbf{M}$ , coil sensitivity operator  $\mathbf{R}$
- 2 **Parameters:**

$$\Theta = \{\gamma, \mathbf{W}_{\{\theta, \phi, \alpha, \beta\}}, \mathbf{D}, \{\mathbf{A}^{H(k)}, \mathbf{B}^{(k)}, \tau_{\{0,1\}}^{(k)}\}_{0=1}^{K-1}\}$$
- 3 **Preprocess:**  $\tilde{\mathbf{y}} = \mathbf{R}^H \mathbf{F}^H \mathbf{y} - \mu$ ,  $\mu = \text{mean}(\mathbf{R}^H \mathbf{F}^H \mathbf{y})$
- 4 **Initialize:**  $\mathbf{z}^{(0)} = \mathbf{0}$ ,  $\Gamma^{(0)} = \mathbf{I}$ ,  $\tau^{(k)} = \tau_0^{(k)} + \hat{\sigma} \tau_1^{(k)} \forall k$
- 5 **for**  $k = 0, 1, \dots, K-1$  **do**
  - 6 //Update Adj. using Alg 4
  - 7  $\Gamma^{(k)} \leftarrow \text{AdjUpdate}(\Gamma^{(k-1)}, \mathbf{z}^{(k)}, \gamma)$
  - 8  $\mathbf{v} = \mathbf{A}^{H(k)} (\mathbf{R}^H \mathbf{F}^H \mathbf{M} \mathbf{F} \mathbf{R} \mathbf{B}^{(k)} \mathbf{z}^{(k)} - \tilde{\mathbf{y}})$
  - 9  $\mathbf{z}^{(k+1)} = \text{GT}_{\tau^{(k)}}(\mathbf{z}^{(k)} - \mathbf{v}; \Gamma^{(k)})$  //Eq. (11)
- 10 **Output:**  $\hat{\mathbf{x}} = \mathbf{D} \mathbf{z}^{(K)} + \mu$

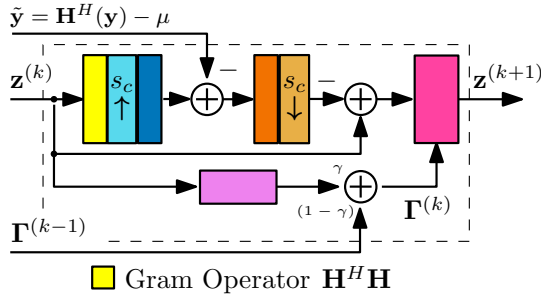


Fig. 4: Block diagram of a single GroupCDL layer in Fig. 2 extended to general linear inverse problem  $\mathbf{y} = \mathbf{H}\mathbf{x} + \nu$ . The layer differs from the denoising GroupCDL by adjoint operator preprocessing and use of the Gram Operator  $\mathbf{H}^H \mathbf{H}$  in each layer. In the case of CS-MRI, the observation operator is a masked multi-coil Fourier transform following a sensitivity map operator,  $\mathbf{H} = \mathbf{M} \mathbf{F} \mathbf{R}$ . Other blocks correspond with Figure 2.

modeled as being contaminated by i.i.d. complex additive Gaussian noise with noise-covariance matrix  $\Sigma \in \mathbb{C}^{C \times C}$ . This observation model may be simplified by considering a coil-whitening pre-processing transformation, resulting in the noise following a diagonal covariance matrix of equal power in each coil, i.e.  $\nu \sim \mathcal{CN}(0, \sigma^2 \mathbf{I})$ . After coil-whitening, the CS-MRI convolutional dictionary BPDN functional takes the form,

$$\underset{\mathbf{z}}{\text{minimize}} \quad \frac{1}{2} \|\mathbf{y} - \mathbf{M} \mathbf{F} \mathbf{R} \mathbf{D} \mathbf{z}\|_2^2 + \lambda \psi(\mathbf{z}). \quad (13)$$

We derive the CS-MRI GroupCDL (and CS-MRI CDL-Net) architectures as a directly parameterized unrolling of PGM applied to (13), employing complex-valued filterbanks/dictionaries. Inverse DFT and coil-combination are applied to the input Fourier domain signal, along with mean-subtraction pre-processing. Correspondingly, the observation Gram operator  $\mathbf{R}^H \mathbf{F}^H \mathbf{M} \mathbf{F} \mathbf{R}$  is inserted after synthesis convolution in each layer. These changes are summarized in Algorithm 6 and Figure 4.

Whereas the standard i.i.d. denoising problem involves a purely local (pixel-wise) image degradation, CS-MRI represents a global image degradation via aliasing artifacts.

Circulant-Sparse Attention is especially well suited for tackling the CS-MRI as global aliasing artifacts can be taken into account via joint inference over the entire image with attention computations seamlessly centered on each pixel of interest. In contrast, patch-based dense attention arbitrarily divides its field of view, limiting its modeling capabilities for global degradation operators.

#### D. Computational Burden of Patch-based Dense Attention

The circulant-sparse attention employed by GroupCDL is favorable to the patch-based dense attention employed by GroupSC [2] and black-box DNNs [6], [7], because it naturally encourages agreement on overlapping regions and centers the attention windows on each pixel. As shown in Figure 1a, patch-based dense attention may additionally incur computational overhead by processing overlapping pixels multiple times. Let  $N = N_1 \times N_2$  be the number of pixels in an image processed by window-size  $W \times W$  (for both patch-attention and CircAtt), and denote window-stride  $s_w \times s_w$ . We express the burden factor as a ratio of the number of pixels processed by a single patch-based dense attention layer over a CircAtt layer,

$$\frac{N_1/s_w \times N_2/s_w \times W^2}{N_1 \times N_2} = \frac{W^2}{s_w^2}. \quad (14)$$

Common nonlocal window sizes,  $45 \times 45$ , and window-strides,  $7 \times 7$ , such as used by NLRN [6], make this burden factor 41 times the computational complexity of an equivalent CircAtt implementation. GroupCDL's use of strided convolution may add an additional  $s_w^2 \times$  computational benefit compared to common NLSS implementations by computing similarities over a reduced spatial dimension  $Q = N/s_w^2$ .

Note that shifted-window (Swin) attention (employed by SwinIR [7]) side-steps this burden factor by patching without overlap ( $s_w = W$ ) twice (successively) with shifted patch boundaries. Swin attention may also enjoy enhanced processing speeds due to its use of dense-array arithmetic vs. CircAtt's use of sparse-array arithmetic. Yet, Swin attention does not address the modeling deficiencies inherent with patch-based dense attention. This is demonstrated in experimentally by GroupCDL's on-par performance with SwinIR at a fraction of its learned parameter count, in Section IV-B.

We further explore the relation between computation time and denoising performance of patch-based dense attention vs CircAtt in the Supplementary Material.

#### E. Group-Thresholding vs. Black-box Attention

Nonlocal self-similarity is used across domains in DNNs, from transformer architectures [24] to nonlocal image restoration networks [6], [7]. The underlying formula behind these methods is most commonly dot-product attention (DPA), easily expressed in terms of the reshaped latent  $\mathbf{Z} \in \mathbb{R}^{N \times M_{\text{in}}}$  as,

$$\begin{aligned} \mathbf{K} &= \mathbf{Z}^{(k)} \mathbf{W}_k^T, & \mathbf{Q} &= \mathbf{Z}^{(k)} \mathbf{W}_q^T, & \mathbf{V} &= \mathbf{Z}^{(k)} \mathbf{W}_v^T \\ \Gamma &= \text{row-sm}(\mathbf{K} \mathbf{Q}^T) \\ \mathbf{Z}^{(k+1)} &= \Gamma \mathbf{V} \end{aligned} \quad (15)$$

TABLE II: Architectures of the GroupCDL models, CDLNet models, and variants presented in the experimental section. Conv-stride  $s_c = 2$  for all models.

Name	Task	$p$	$K$	$M$	$M_h$	$W$	$\Delta K$
CDLNet	Denoise	7	30	169	-	-	-
GroupCDL	Denoise, CS-MRI	7	30	169	64	35	5
Big-GroupCDL	Denoise	9	40	448	128	45	10

where  $\mathbf{W}_q, \mathbf{W}_k \in \mathbb{R}^{M_h \times M_{in}}$ ,  $\mathbf{W}_v \in \mathbb{R}^{M_{out} \times M_{in}}$ , and  $\mathbf{Z}^{(k+1)} \in \mathbb{R}^{N \times M_{out}}$ .

Both DPA and the proposed GT (11) make use of a normalized adjacency matrix ( $\Gamma$ ), computed in an asymmetric feature domain<sup>5</sup>. Both use this adjacency to weight the current spatial features, identically over channels. However, in DPA, the weighting directly results in the layer’s output (via matrix multiplication), whereas in GT this weighting informs a spatially adaptive soft-thresholding (see Figure 3).

The proposed GT’s decoupling of adjacency application and output dimension is key in allowing group-thresholding to be computationally efficient, as the adjacency matrix-vector multiplication can be performed over transformed features with a reduced dimension. In contrast, DPA operating with reduced channel dimensions ( $M_{out} \ll M_{in}$ ) would harm the capacity of the network’s latent representation. In Section IV-D we show empirical evidence for favoring the distance similarity in GT over the dot-product similarity of DPA.

#### IV. EXPERIMENTAL RESULTS

##### A. Natural Image Denoising Experimental Setup

**Architecture:** We denote the network detailed in Algorithm 5 as GroupCDL. GroupCDL and CDLNet are trained with noise-adaptive thresholds ( $\tau^{(k)} = \tau_0^{(k)} + \hat{\sigma}\tau_1^{(k)}$ ) unless specified using the -B suffix, indicating the models are noise-blind ( $\tau^{(k)} = \tau_0^{(k)}$ ). The hyperparameters for these architectures are given in Table II, unless otherwise specified.

**Dataset and Training:** Let  $f_\Theta$  denote the GroupCDL DNN as a function of parameters  $\Theta$ . Let  $\mathcal{D} = \{(\mathbf{y}, \sigma, \mathbf{x})\}$  denote a dataset of noisy and ground-truth natural image pairs, with noise-level  $\sigma$ . Grayscale image denoising GroupCDL models were trained on the BSD432 [28] dataset. Grayscale Big-GroupCDL models were additionally trained on the Waterloo Exploration dataset and DIV2K dataset. All models were trained with a supervised mean squared error (MSE) loss,

$$\begin{aligned} & \underset{\substack{\mathbf{W}_\theta, \mathbf{W}_\phi, \mathbf{W}_\alpha, \\ \mathbf{W}_\beta \geq 0, \gamma \in [0, 1], \\ \mathcal{D} \in \mathcal{C}, \{\tau^{(k)} \geq 0\}_{k=0}^{K-1}, \\ \{\mathbf{A}^{(k)} \in \mathcal{C}, \mathbf{B}^{(k)} \in \mathcal{C}\}_{k=0}^{K-1}}}{\text{minimize}} \sum_{\{\mathbf{y}, \sigma, \mathbf{x}\} \in \mathcal{D}} \|f_\Theta(\mathbf{y}, \sigma) - \mathbf{x}\|_2^2, \quad (16) \end{aligned}$$

where  $\mathcal{C} = \{\mathbf{D} : \|\mathbf{D}_{:j}\|_2^2 \leq 1 \ \forall j\}$ . We use the Adam optimizer with default parameters [29], and project the network parameters onto their constraint sets after each gradient step. The dataset is generated online from clean images via random crops, rotations, flips, and AWGN of noise-level  $\sigma$  sampled uniformly within  $\sigma^{\text{train}}$  for each mini-batch element. A mini-batch size of 12 was used. Initial learning-rates of  $5 \times 10^{-4}$

and  $3 \times 10^{-4}$  were used for GroupCDL and Big-GroupCDL, respectively, with cosine-annealing [30] to a final value of  $2 \times 10^{-6}$ . Each network was trained for  $\approx 600k$  gradient steps. Additional training hyperparameter details (such as backtracking) follow the CDLNet setup [1].

Test and validation performance is evaluated on several datasets. The dataset name, along with (arithmetic) average dimensions, are provided to better understand reported inference timings: Set12 ( $362 \times 362$ ), CBS68 [28] ( $481 \times 321$ ), Urban100 [31] ( $1030 \times 751$ ), and NikoSet10<sup>6</sup> ( $1038 \times 779$ ).

**Training Initialization:** GroupCDL models are initialized as ISTA<sup>7</sup> with  $\tau_0 = 10^{-3}$ ,  $\tau_1 = 0$ , and a base dictionary  $\mathbf{D}$  that has been spectrally normalized. Details are given in [1]. Pixel-wise transforms  $\mathbf{W}_{\{\theta, \phi, \alpha, \beta\}}$  are initialized with the same weights drawn from a standard uniform distribution and spectrally-normalized. We initialize parameter  $\gamma = 0.8$ .

**Hardware:** All models were trained on a single core Intel Xeon CPU with 2.90 GHz clock and a single NVIDIA A100 GPU. GroupCDL training takes approximately 48 hours. For code-base compatibility reasons, inference timings for methods (GroupCDL, GroupSC, NLRN, GCDN) in Tables III were determined by running models on NVIDIA Quadro RTX-8000, whereas for other listed methods (Big-GroupCDL, SwinIR, Restormer, DCDicl) we report NVIDIA A100 inference time.

##### B. Single Noise-Level Performance

In this section, we demonstrate competitive denoising performance of the proposed GroupCDL. All models are trained on a single noise-level and tested at the same noise-level ( $\sigma^{\text{train}} = \sigma^{\text{test}}$ ). We compare GroupCDL to its fully convolutional counterpart (CDLNet), patch-processing dictionary learning based nonlocal DNN (GroupSC) [2], and state-of-the-art black-box DNNs [6], [7], [18], [22], [32].

Table III shows the grayscale denoising performance and inference speed of the aforementioned models across several common datasets. We include a learned parameter count as a crude measure of expressivity of the model. The group-sparsity prior of GroupCDL significantly increases denoising performance compared to the unstructured sparsity prior of CDLNet. We observe that GroupCDL has denoising performance superior to other dictionary learning based networks using group sparsity prior (GroupSC) and competitive performance with black-box nonlocal methods GCDN and NLRN. GroupCDL also significantly outperforms these methods in inference time due to the computational efficiency of CircAtt over overlapping patch-based dense attention. Big-GroupCDL is shown to outperform GCDN and be competitive with state-of-the-art black-box networks SwinIR, Restormer, and DCDicl, with on par inference time and only a fraction of the learned parameters.

Figure 5 highlights the qualitative differences between Big-GroupCDL and state-of-the-art black-box networks (SwinIR [7], Restormer [22]). We observe that Big-GroupCDL is able to produce denoised images on par with SwinIR and Restormer (Fig. 5 first row red box), and may even retain a greater amount

<sup>6</sup>see <https://github.com/nikopj/GroupCDL>.

<sup>7</sup> $(\mathbf{A}^{(k)} = \mathbf{B}^{(k)} = \mathbf{D} \ \forall k)$

<sup>5</sup> $(\mathbf{W}_k \neq \mathbf{W}_q, \mathbf{W}_\theta \neq \mathbf{W}_\phi)$



TABLE III: Grayscale denoising performance (PSNR (dB)/ 100×SSIM) and GPU inference runtimes. All learned methods are trained for individual noise-levels ( $\sigma = \sigma^{\text{train}} = \sigma^{\text{test}}$ ). Learned parameter counts are displayed below the method names.

Dataset	Noise $\sigma$	CDLNet 507k [1]	GroupSC 68k [2]	NLRN 340k [6]	GroupCDL 550k	GCDN 6M [32]	SwinIR 11M [7]	Restormer 25M [22]	DCDiL 33M [18]	Big-GroupCDL 3M
Set12	15	32.87/90.43	32.85/90.63	33.16/90.70	33.05/90.73	33.14/90.72	33.36/91.11	33.42/91.28	33.34/91.15	33.24/91.02
	25	30.52/86.55	30.44/86.42	30.80/86.89	30.75/86.93	30.78/86.87	31.00/87.38	31.08/87.64	31.03/87.48	30.91/87.35
	50	27.42/79.41	27.14/77.97	27.64/79.80	27.63/80.04	27.60/79.57	27.87/80.84	27.95/81.18	28.00/81.22	27.85/80.82
time (s)		0.019	22.07	25.62	0.68	405	1.88	0.13	0.42	1.60
BDS68 [28]	15	31.74/89.18	31.70/89.63	31.88/89.32	31.82/89.41	31.70/89.63	31.96/89.60	31.96/89.65	31.95/89.57	31.90/89.57
	25	29.26/83.06	29.20/83.36	29.41/83.31	29.38/83.51	29.35/83.32	29.50/83.77	29.52/83.90	29.52/83.79	29.46/83.76
	50	26.35/72.69	26.17/71.83	26.47/72.98	26.47/73.32	26.38/73.89	26.57/73.79	26.60/73.99	26.63/73.95	26.57/73.83
time (s)		0.022	23.63	26.66	0.65	540	1.43	0.14	0.38	1.67
Urban100 [31]	15	32.59/92.85	32.72/93.08	33.42/93.48	33.07/93.40	33.47/93.58	33.75/93.98	33.79/94.09	33.59/93.88	33.56/93.89
	25	30.03/89.00	30.05/89.12	30.88/90.03	30.61/90.03	30.95/90.20	31.30/90.94	31.46/91.29	31.30/91.08	31.20/90.93
	50	26.66/81.11	26.43/80.02	27.40/82.44	27.29/83.05	27.41/81.60	28.05/84.84	28.29/85.60	28.24/85.49	28.03/84.83
time (s)		0.090	93.33	135.8	3.56	1580	4.98	0.60	1.75	8.32

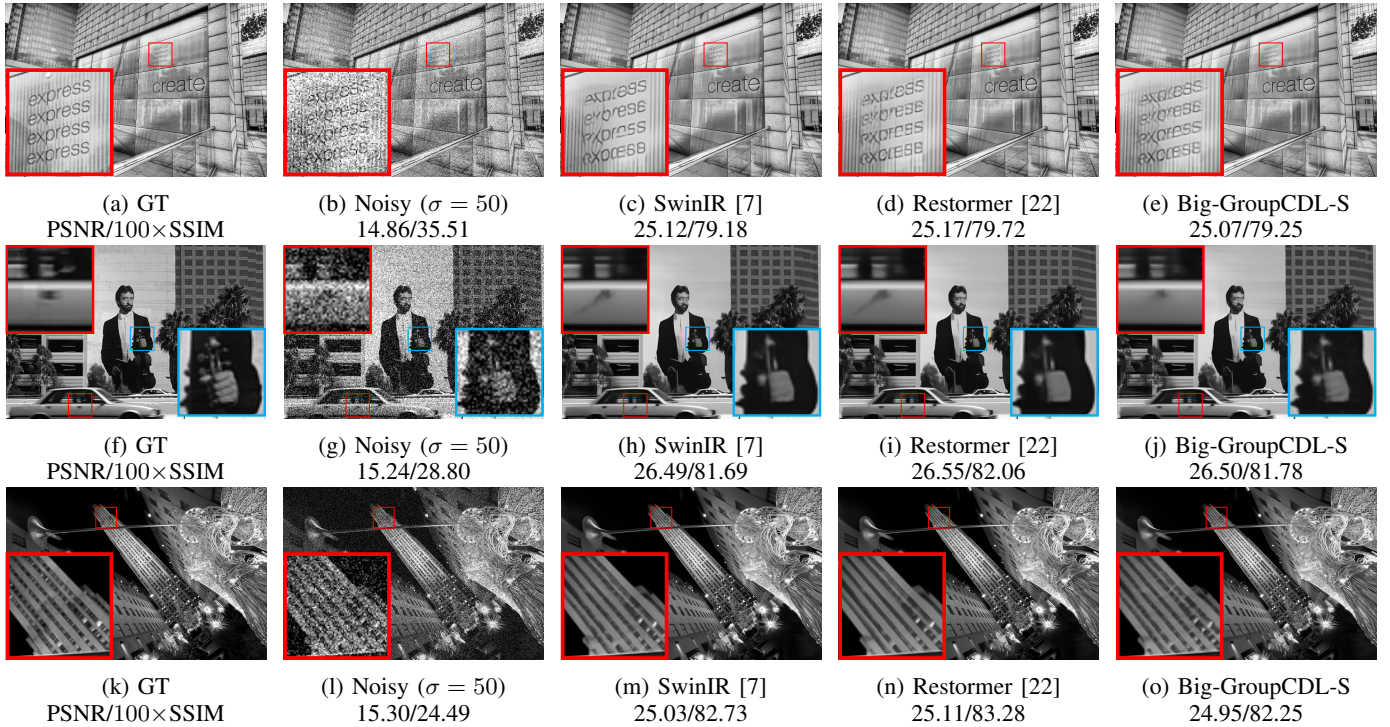


Fig. 5: Visual comparison of large parameter count deep denoisers.

of detail information where SwinIR and Restormer appear to over-smooth detailed regions (Fig. 5 second row red box, third row red box) or hallucinate image structures (Fig. 5 second row blue box).

### C. Noise-Level Generalization

Figure 6 shows that the proposed novel group-thresholding scheme (11) is able to obtain near-perfect noise-level generalization (w.r.t GroupCDL-S performance). This serves as empirical evidence for the interpretation of the unrolled network as performing some approximate/accelerated group-sparse BPDN, as the noise-adaptive thresholds ( $\tau = \tau_0 + \hat{\sigma}\tau_1$ ;  $\hat{\sigma}$  estimated following [1]) appear to correspond very well to their classical counter-parts from which they are derived.

Figure 6 also shows a single input nonlocal window  $y$  across noise-levels  $\sigma$  and the computed adjacency values of the three types of GroupCDL models (GroupCDL-S, GroupCDL-B, GroupCDL). The adjacency visualizations of GroupCDL-B

show a catastrophic failure in the similarity computations of the network above  $\sigma^{\text{train}}$ , as no structure is found. Similar patterns are seen in the GroupCDL models (with noise-adaptive thresholds) compared to those of GroupCDL-S.

### D. Ablation Studies

In this section we examine the denoising and inference time performance of the GroupCDL model under different hyper-parameters associated with the proposed group-thresholding operation (11), (10). Table IV shows the effect of the update-interval parameter ( $\Delta K$ ), which determines how often we update the adjacency  $\Gamma^{(k)}$  in the network (every  $\Delta K$  layers, see Alg. 5). We observe that decreasing the update interval increases denoising performance, with diminishing returns, at cost to the inference speed of the network.

Table V shows the effect of employing learned pixel-wise transforms in the similarity computation (10) ( $W_\theta, W_\phi$ ) and group-thresholding (11) ( $W_\alpha, W_\beta$ ). The table also shows

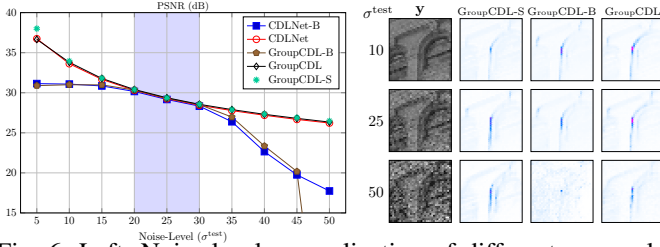


Fig. 6: Left: Noise-level generalization of different grayscale denoising networks based on BSD68 [28]. GroupCDL-S is trained at  $\sigma^{\text{test}}$  for each point on the graph. All other networks are trained on  $\sigma^{\text{train}} = [20, 30]$ . Right: Visualization of normalized adjacency  $\Gamma_i^{(K)}$  for  $i$ th pixel of input image ( $\mathbf{y}$ ) at noise-levels  $\sigma = 10, 25, 50$ . Catastrophic failure of GroupCDL-B model is observed for  $\sigma > \sigma^{\text{train}}$ .

TABLE IV: Effect of update interval ( $\Delta K$ ). Grayscale denoising performance averaged over the NikoSet10 dataset ( $\sigma^{\text{train}} = \sigma^{\text{test}} = 25$ ).

$\Delta K$	PSNR/100×SSIM	time (s)
2	30.22/86.88	4.01
3	30.22/86.87	4.72
5	30.21/86.87	3.47
10	30.21/86.87	3.24
15	30.19/86.79	3.18

the effect of employing channel reduction in these transforms ( $M_h \ll M = 169$ ) and a comparison of using the distance similarity (Alg. 1) vs. dot-product similarity (Alg. 3). We observe that pixel-wise transforms increases denoising performance. Furthermore, setting  $M_h \ll M$  roughly preserves the performance, while greatly reducing the inference time, with the reduction roughly equal to the channel reduction ratio  $M/M_h = 169/64 \approx 8.89/3.47$ . This demonstrates one advantage of group-thresholding over black-box dot-product attention: the dimension for similarity calculation and attention operation ( $M_h$ ) is decoupled from the layer’s output channel dimension and may be tuned to achieve a better trade-off between speed and performance. Distance-similarity is also empirically shown to achieve better performance over dot-product similarity.

### E. Application to Compressed-Sensing MRI

In this section, we apply the GroupCDL architecture (detailed in Section III-C) to supervised training for the CS-MRI problem, with and without noise contamination.

**Experimental Setup:** We use the fully-sampled MoDL multi-coil brain dataset [36], which was acquired using a 3D T2 CUBE sequence with an isotropic 1 mm resolution, a 210 mm × 210 mm field-of-view, and echo-time of 84 ms. The dataset contains 360 slices for training and 164 for testing. Sensitivity maps are provided by the dataset. We follow the experimental setup of [37] by using random Cartesian Fourier domain subsampling (in a single readout direction) for 4× and 8× acceleration with 8% and 4% of center lines preserved, respectively.

**Training:** We train CDLNet and GroupCDL models for CS-MRI using identical model and training hyperparameters as

TABLE V: Effect of NLSS feature compression. Grayscale denoising performance averaged over the NikoSet10 dataset ( $\sigma^{\text{train}} = \sigma^{\text{test}} = 25$ ).

feature-compression	$M_h$	sim_fun	PSNR/100×SSIM	time (s)
none	n/a	distance	30.19/86.79	8.64
$\mathbf{W}_{\{\theta, \phi\}}$	64	distance	30.21/86.86	8.13
$\mathbf{W}_{\{\theta, \phi, \alpha, \beta\}}$	169	distance	30.21/86.89	8.89
$\mathbf{W}_{\{\theta, \phi, \alpha, \beta\}}$	64	distance	30.21/86.87	3.47
$\mathbf{W}_{\{\theta, \phi, \alpha, \beta\}}$	32	distance	30.20/86.84	2.00
$\mathbf{W}_{\{\theta, \phi, \alpha, \beta\}}$	64	dot	30.11/86.55	3.43

the grayscale denoising models (see Table II), though each filter is now complex-valued (nearly doubling the learned parameter count). Following [37], we replace the standard MSE loss function with an  $\ell_1$  – ssim loss function for fair comparison. PSNR and SSIM computations use a peak-value of 1.0, following [37].

**No Noise:** Table VI shows the results of training the proposed GroupCDL against state-of-the-art deep-learning CS-MRI reconstruction, without the presence of additive noise. Both GroupCDL and CDLNet perform significantly better than state-of-the-art methods. GroupCDL distinguishes itself from CDLNet at the higher acceleration reconstruction. These observations are bolstered in Figure 7 where the black-box DNN HFMRI [37] is shown to have significantly more structure present in their reconstruction error maps compared to GroupCDL.

**With Noise:** Figure 8 shows the results of CS-MRI reconstruction training in the presence of Fourier domain AWGN, across noise-levels. The proposed CS-MRI GroupCDL model was trained for 4× reconstruction on an intermediate noise-range ( $\sigma^{\text{train}} = [0.08, 0.12]$ )<sup>8</sup>. Such a training may be encountered in practice where ground-truth images are unavailable and the limited available data is corrupted with varying noise-levels. Figure 8b shows that GroupCDL’s noise-adaptive thresholds enable effective inference both above and below the training noise-range. Figure 8’s visual examples show that GroupCDL-B is unable to adequately recover features/textures below the training noise-range, and introduces severe artifacts above it. In contrast, GroupCDL (with noise-adaptive thresholds) is able to recover additional image details below the training range, and generalize gracefully above it.

## V. DISCUSSION AND CONCLUSION

In GroupCDL, we adapt the classical, patch-processing based, group-sparsity prior to convolutional sparse coding (CSC) and apply it to the direct-parametrization unrolling frame-work of CDLNet [1]. In doing so, we arrive at a sliding-window NLSS consistent with the CSC model (CircAtt), which addresses the modeling pitfalls of patch-based dense attention. We demonstrate competitive denoising performance to state-of-the-art black-box networks with notable efficiency in the number of learned parameters. We show that the CircAtt operation allows GroupCDL to be easily and effectively extended to global degradation operator inverse-problems such as CS-MRI. GroupCDL brings substantial gain over current

<sup>8</sup>with an image-domain maximum magnitude of 1.6



TABLE VI: CS-MRI reconstruction performance (PSNR (dB)/100×SSIM) . All learned methods are trained on the MoDL Brain dataset [36]. Learned parameter counts are displayed below the method names. \*Numbers reported in [37].

Accel.	Zero-Filled	MoDL* [36]	ISTA-Net+* [38]	VS-Net* [39]	HFMRI* [37]	CDLNet	GroupCDL
	-	5.6M	368k	1.0M	1.1M	1.0M	1.1M
4x	25.60/80.61	28.89/80.1	32.26/91.6	32.18/91.4	33.20/93.8	<b>36.20/96.01</b>	<b>36.55/95.97</b>
8x	23.24/72.91	25.28/71.1	27.48/83.1	27.56/83.3	27.65/85.3	<u>29.93/89.47</u>	<b>30.49/89.94</b>

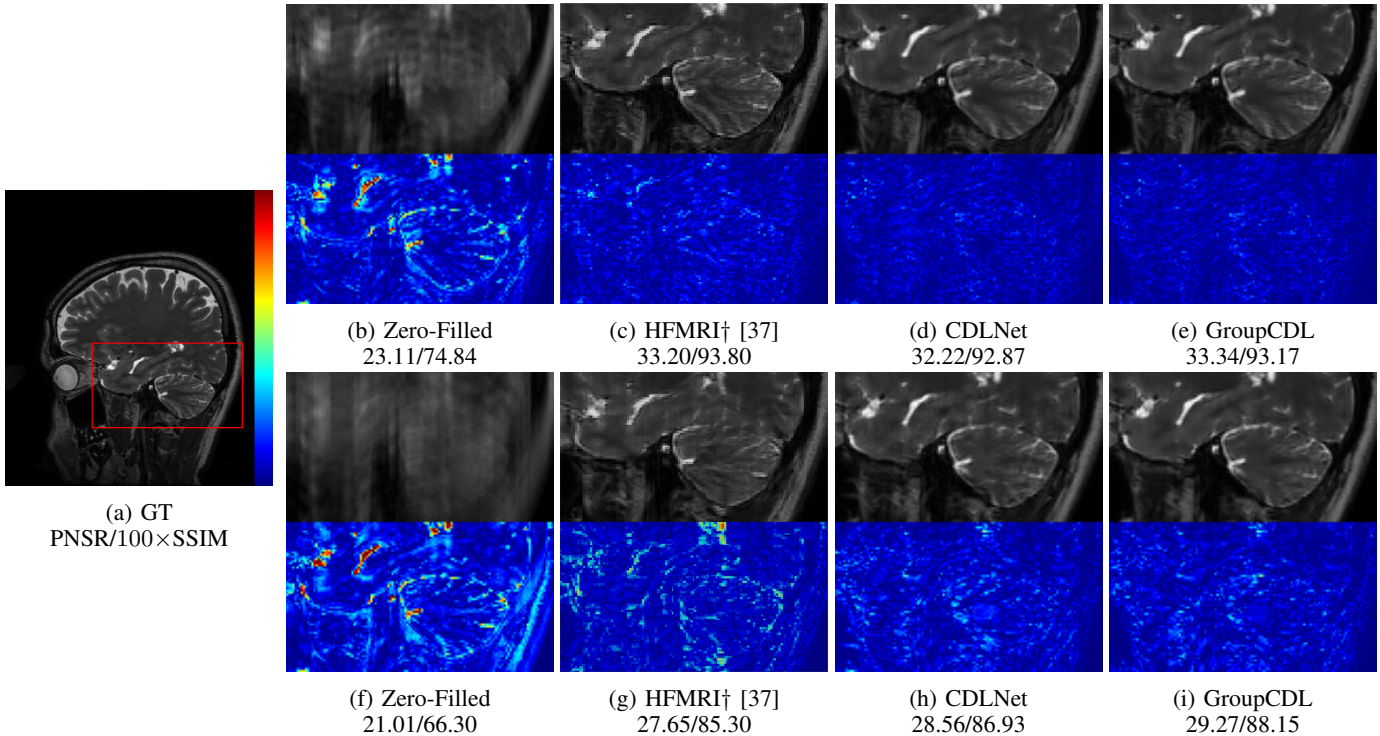


Fig. 7: Visual comparison of multi-coil CS-MRI reconstruction models on a selected crop of slice 111 from the MODL Brain test set [36]. Magnitude error maps shown below each crop. Top-row: 4x acceleration. Bottom-row: 8x acceleration. †figure and numbers taken from [37].

state-of-the-art black-box nonlocal networks for CS-MRI in the case of zero-noise reconstruction.

Additionally, GroupCDL inherits the noise-level generalization capabilities of CDLNet [1]. This robustness to training-inference mismatch may be of special interest to practical scenarios, where ground-truth is unavailable and inference noise-levels may deviate from what is present in a training dataset. We leverage GroupCDL’s noise-adaptive thresholds to recover image details especially well in such cases. To the best of our knowledge, robustness to training-inference noise-level mismatch for CS-MRI has not been considered in prior literature.

When scaled up, GroupCDL performs very competitively with state-of-the-art black-box DNNs, even without incorporating existing state-of-the-art modeling choices such as multi-resolution processing and transposed-attention. Future work may consider additionally incorporating these features into the GroupCDL framework to enable even better performance and inference speeds. We believe GroupCDL’s interpretability and robustness are well suited to tackle other large signal reconstruction problems with nonlocal image-domain artifacts, especially in the unsupervised learning regime.

#### ACKNOWLEDGMENTS

The authors would like to thank NYU HPC for its computing resources and technical support. The authors are grateful to Che Maria Baez for her linguistic revisions on a preliminary draft of this manuscript.

#### REFERENCES

- [1] N. Janjušević, A. Khalilian-Gourtani, and Y. Wang, “CDLNet: Noise-adaptive convolutional dictionary learning network for blind denoising and demosaicing,” *IEEE Open Journal of Signal Processing*, vol. 3, pp. 196–211, 2022.
- [2] B. Lecouat, J. Ponce, and J. Mairal, “Fully trainable and interpretable non-local sparse models for image restoration,” in *European Conference on Computer Vision (ECCV)*, 2020.
- [3] N. Janjušević, A. Khalilian-Gourtani, and Y. Wang, “Gabor is enough: Interpretable deep denoising with a gabor synthesis dictionary prior,” in *2022 IEEE 14th Image, Video, and Multidimensional Signal Processing Workshop (IVMSP)*, 2022, pp. 1–5.
- [4] D. Simon and M. Elad, “Rethinking the CSC model for natural images,” in *Advances in Neural Information Processing Systems*, 2019, pp. 2274–2284.
- [5] M. Scetbon, M. Elad, and P. Milanfar, “Deep k-svd denoising,” *IEEE Transactions on Image Processing*, vol. 30, pp. 5944–5955, 2019.
- [6] D. Liu, B. Wen, Y. Fan, C. C. Loy, and T. S. Huang, “Non-local recurrent network for image restoration,” in *Advances in Neural Information Processing Systems*, 2018, pp. 1680–1689.

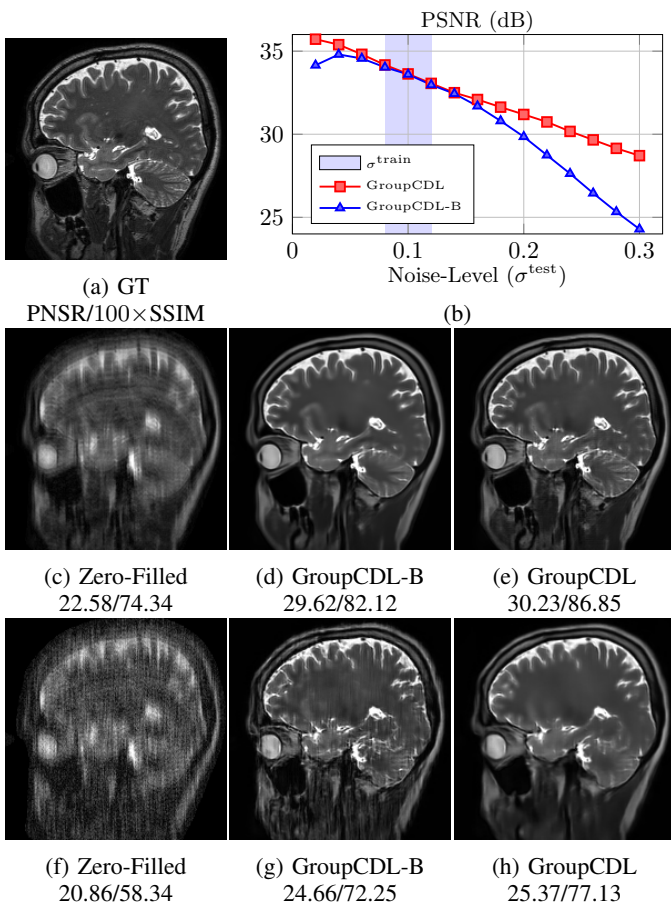


Fig. 8: Visual comparison of Joint-Denoising and CS-MRI reconstruction models with (GroupCDL) and without noise-adaptive thresholds (GroupCDL-B) on MODL Brain test set [36]. Each model was trained for  $4\times$  acceleration on a noise-range  $\sigma^{\text{train}} \in [0.08, 0.12]$ . Top-row:  $\sigma^{\text{test}} = 0.02$ . Bottom-row:  $\sigma^{\text{test}} = 0.25$ .

[7] J. Liang, J. Cao, G. Sun, K. Zhang, L. Van Gool, and R. Timofte, “Swinir: Image restoration using swin transformer,” in *Proceedings of the IEEE/CVF International Conference on Computer Vision (ICCV) Workshops*, October 2021, pp. 1833–1844.

[8] J. Bezanson, A. Edelman, S. Karpinski, and V. B. Shah, “Julia: A fresh approach to numerical computing,” *SIAM Review*, vol. 59, no. 1, pp. 65–98, 2017. [Online]. Available: <https://doi.org/10.1137/141000671>

[9] S. Mallat, *A Wavelet Tour of Signal Processing: The Sparse Way*. Elsevier Science, 2008.

[10] A. Beck and M. Teboulle, “A fast iterative shrinkage-thresholding algorithm for linear inverse problems,” *SIAM Journal on Imaging Sciences*, vol. 2, pp. 183–202, 01 2009.

[11] J. Mairal, F. Bach, J. Ponce, G. Sapiro, and A. Zisserman, “Non-local sparse models for image restoration,” in *Proceedings of 12th IEEE International Conference on Computer Vision (ICCV)*, 2009, pp. 2272–2279.

[12] J. Mairal, F. Bach, J. Ponce, and G. Sapiro, “Online dictionary learning for sparse coding,” in *Proceedings of the 26th International Conference on Machine Learning (ICML)*, 2009, pp. 689–696.

[13] G. Ongie, A. Jalal, C. A. Metzler, R. G. Baraniuk, A. G. Dimakis, and R. Willett, “Deep learning techniques for inverse problems in imaging,” *IEEE Journal on Selected Areas in Information Theory*, vol. 1, no. 1, pp. 39–56, 2020.

[14] D. Gilton, G. Ongie, and R. Willett, “Neumann networks for linear inverse problems in imaging,” *IEEE Transactions on Computational Imaging*, vol. 6, pp. 328–343, 2019.

[15] —, “Deep equilibrium architectures for inverse problems in imaging,”

*IEEE Transactions on Computational Imaging*, vol. 7, pp. 1123–1133, 2021.

[16] O. Ronneberger, P. Fischer, and T. Brox, “U-Net: Convolutional networks for biomedical image segmentation,” *Medical Image Computing and Computer-Assisted Intervention*, p. 234–241, 2015.

[17] K. He, X. Zhang, S. Ren, and J. Sun, “Deep residual learning for image recognition,” in *Proceedings of the IEEE conference on computer vision and pattern recognition*, 2016, pp. 770–778.

[18] H. Zheng, H. Yong, and L. Zhang, “Deep convolutional dictionary learning for image denoising,” in *Proceedings of the IEEE/CVF Conference on Computer Vision and Pattern Recognition (CVPR)*, June 2021, pp. 630–641.

[19] H. Sreter and R. Giryes, “Learned convolutional sparse coding,” in *Proceedings of IEEE International Conference on Acoustics, Speech and Signal Processing (ICASSP)*, 2018, pp. 2191–2195.

[20] K. Gregor and Y. LeCun, “Learning fast approximations of sparse coding,” in *Proceedings of the 27th International Conference on Machine Learning (ICML)*, 2010, pp. 399–406.

[21] Z. Liu, Y. Lin, Y. Cao, H. Hu, Y. Wei, Z. Zhang, S. Lin, and B. Guo, “Swin transformer: Hierarchical vision transformer using shifted windows,” in *Proceedings of the IEEE/CVF International Conference on Computer Vision (ICCV)*, 2021.

[22] S. W. Zamir, A. Arora, S. Khan, M. Hayat, F. S. Khan, and M.-H. Yang, “Restormer: Efficient transformer for high-resolution image restoration,” in *CVPR*, 2022.

[23] R. Child, S. Gray, A. Radford, and I. Sutskever, “Generating long sequences with sparse transformers,” URL <https://openai.com/blog/sparse-transformers>, 2019.

[24] T. Dao, D. Y. Fu, S. Ermon, A. Rudra, and C. Ré, “FlashAttention: Fast and memory-efficient exact attention with IO-awareness,” in *Advances in Neural Information Processing Systems*, 2022.

[25] Y. Mei, Y. Fan, and Y. Zhou, “Image super-resolution with non-local sparse attention,” in *Proceedings of the IEEE/CVF Conference on Computer Vision and Pattern Recognition (CVPR)*, June 2021, pp. 3517–3526.

[26] D. Khashabi, S. Nowozin, J. Jancsary, and A. W. Fitzgibbon, “Joint demosaicing and denoising via learned nonparametric random fields,” *IEEE Transactions on Image Processing*, vol. 23, pp. 4968–4981, 2014.

[27] T. Besard, C. Foket, and B. De Sutter, “Effective extensible programming: Unleashing Julia on GPUs,” *IEEE Transactions on Parallel and Distributed Systems*, 2018.

[28] D. Martin, C. Fowlkes, D. Tal, and J. Malik, “A database of human segmented natural images and its application to evaluating segmentation algorithms and measuring ecological statistics,” in *Proceedings of 8th IEEE International Conference on Computer Vision (ICCV)*, vol. 2, 2001, pp. 416–423.

[29] D. P. Kingma and J. Ba, “Adam: A method for stochastic optimization,” in *International Conference on Learning Representations (ICLR)*, 2015.

[30] I. Loshchilov and F. Hutter, “Sgdr: Stochastic gradient descent with warm restarts,” *arXiv preprint arXiv:1608.03983*, 2016.

[31] J.-B. Huang, A. Singh, and N. Ahuja, “Single image super-resolution from transformed self-exemplars,” in *Proceedings of the IEEE Conference on Computer Vision and Pattern Recognition (CVPR)*, June 2015.

[32] D. Valsesia, G. Fracastoro, and E. Magli, “Deep graph-convolutional image denoising,” *IEEE Transactions on Image Processing*, vol. 29, pp. 8226–8237, 2020.

[33] K. Dabov, A. Foi, V. Katkovnik, and K. Egiazarian, “Image denoising by sparse 3-D transform-domain collaborative filtering,” *IEEE Transactions on Image Processing*, vol. 16, no. 8, pp. 2080–2095, 2007.

[34] K. Zhang, W. Zuo, Y. Chen, D. Meng, and L. Zhang, “Beyond a gaussian denoiser: Residual learning of deep CNN for image denoising,” *IEEE Transactions on Image Processing*, vol. 26, no. 7, p. 3142–3155, 2017.

[35] P. Liu, H. Zhang, K. Zhang, L. Lin, and W. Zuo, “Multi-level wavelet-cnn for image restoration,” *2018 IEEE/CVF Conference on Computer Vision and Pattern Recognition Workshops (CVPRW)*, Jun 2018. [Online]. Available: <http://dx.doi.org/10.1109/CVPRW.2018.00121>

[36] H. K. Aggarwal, M. P. Mani, and M. Jacob, “Modl: Model-based deep learning architecture for inverse problems,” *IEEE Transactions on Medical Imaging*, vol. 38, no. 2, pp. 394–405, 2019.

[37] J. Liu, C. Qin, and M. Yaghoobi, “High-fidelity mri reconstruction using adaptive spatial attention selection and deep data consistency prior,” *IEEE Transactions on Computational Imaging*, vol. 9, pp. 298–313, 2023.

[38] J. Zhang and B. Ghanem, “Ista-net: Interpretable optimization-inspired deep network for image compressive sensing,” in *2018 IEEE/CVF Conference on Computer Vision and Pattern Recognition*, 2018, pp. 1828–1837.

- [39] J. Duan, J. Schlemper, C. Qin, C. Ouyang, W. Bai, C. Biffi, G. Bello, B. Statton, D. P. O'Regan, and D. Rueckert, "Vs-net: Variable splitting network for accelerated parallel mri reconstruction," in *Medical Image Computing and Computer Assisted Intervention – MICCAI 2019*, D. Shen, T. Liu, T. M. Peters, L. H. Staib, C. Essert, S. Zhou, P.-T. Yap, and A. Khan, Eds. Cham: Springer International Publishing, 2019, pp. 713–722.